Journal of Photochemistry and Photobiology A: Chemistry 225 (2011) 125–134

Contents lists available at SciVerse ScienceDirect

Journal of Photochemistry and Photobiology A: Chemistry

journal homepage: www.elsevier.com/locate/jphotochem

Fluorescence resonance energy transfer and arrangements of fluorophores in integrated coumarin/cyanine systems within solid-state two-dimensional nanospace

Kazuko Fujii*, Takashi Kuroda, Kazuaki Sakoda, Nobuo Iyi

National Institute for Materials Science (NIMS), 1-1 Namiki, Tsukuba, Ibaraki 305-0044, Japan

ARTICLE INFO

Article history:
Received 9 June 2011
Received in revised form 6 September 2011
Accepted 3 October 2011
Available online 10 October 2011

Keywords:
Integrated dyes system
Layered inorganic/organic hybrid
Fluorescence resonance energy transfer
Two-dimensional nanospace
Nano-level structure

ABSTRACT

Two functional dyes, coumarin and 3,3′-diethyloxacarbocyanine (DOC), are integrated with a wide range of DOC contents by intercalating DOC into the solid-state two-dimensional nanospace of a coumarin/phyllosilicate hybrid, wherein the coumarin moiety is anchored covalently to the phyllosilicate moiety. Ultraviolet–visible spectroscopy and X-ray diffraction analysis show that the mole ratios of DOC to coumarin moiety ([DOC]/[Coum]) range from 0.004 to 40 mol/mol, thus providing a series of systems with a variety of fluorescence properties and arrangements of fluorophores. Fluorescence spectroscopy reveals that both the coumarin moieties and DOC molecules fluoresce and that DOC even emits by excitation at 320 nm due to energy transfers within the integrated coumarin/DOC systems. The extent of the energy transfers and fluorescence intensities depend on [DOC]/[Coum]. The proposed models of the arrangements of the fluorophores for the integrated systems consist of coumarin moieties located on both close to and far from the DOC molecules in the same two-dimensional nanospace with the DOC molecules always in close proximity to a coumarin moiety. These unique arrangements of fluorophores allow two types of fluorescence behavior: (1) fluorescence resonance energy transfer (FRET) from the excited coumarin moiety located close to DOC and (2) emission by coumarin for the excited coumarin moiety located far from DOC.

1. Introduction

The advantages of immobilizing multiple substances in the spaces of solid media are that the substances can express diverse functions and that multifunctional solid-state devices can be fabricated. Furthermore, in integrated systems, the distances and orientation between the target reaction substances, including functional dyes, metal complexes, etc., can be fixed [1–50]. The target reactions, such as photoinduced electron transfer and energy transfer (ET), are interesting basic reactions of photosynthesis. Therefore, immobilization has attracted considerable attention in the fields of artificial photosynthesis, photochemistry, hybrid nanomaterial chemistry, etc. Integrated systems have recently been constructed in nano-ordered pore channels of mesoporous organosilicas [1–9], multifilms [10–22], interlayer nanospaces of phyllosilicates [23–38], and others [39–50]. One of the most important objectives of these studies has been to understand the relevance of the nano-level structure to the target reactions and to control the target reactions by designing suitable nano-level structures, e.g., the suitable distances and dispositions of the immobilized target reaction substances [1–5,8,10,11,13,14,16,17,19–32,40,44,45,48,49].

The efficiency of fluorescence resonance energy transfer (FRET) depends strongly on the distance between the donor and acceptor (D–A distance) [1–5,10,12–16,20,23,26,29,32,50,51]. The Förster distance (R_0) is the distance between the donor and the acceptor at which the FRET rate is equal to the emission decay rate from a donor in the absence of an acceptor and is typically in the range of 1.5–9.0 nm [1,2,5,10,12–15,23,51,52]. Dexter-type ET is associated with the electron exchange process and is dominant when the D–A distance is short enough that their electron orbitals overlap [53]. Radiative ET is due to emission from the excited donor and subsequent reabsorption of the photons by the acceptor [51]. FRET and Dexter-type ET exceed radiative ET in cases where the donor–acceptor distance does not significantly exceed R_0. Interesting investigations have been reported on regulating the D–A distances by inserting a spacer in layer-by-layer deposited ET systems [10], changing the spacer chain length in polymers [44,45,49] and supramolecules [40,47], etc. [23,25,28,32].

Two-dimensional nanospace is more effective for the construction of integrated systems than three-dimensional nanospace

* Corresponding author. Tel.: +81 29 860 4363; fax: +81 29 852 7449.
E-mail address: FUJII.Kazuko@nims.go.jp (K. Fujii).

1010-6030/$ – see front matter © 2011 Elsevier B.V. All rights reserved.
doi:10.1016/j.jphotochem.2011.10.009

because it is possible to more concisely analyze how the nano-level structure governs the mechanisms and extent of the target reactions in two-dimensional nanospace. Therefore, the extent of the target reactions can be more easily controlled. Phyllosilicates have layered structures with each layer consisting of two-dimensional Si tetrahedral and cation octahedral sheets [54]. The interlayer spaces in phyllosilicates provide an attractive two-dimensional nanospace, which can be easily expanded to accommodate the height of a guest [24,25,30,36,46]. However, it has been reported that the preparation of integrated systems is difficult because of the stratification of the co-intercalants into individual interlamellar spaces, i.e., segregation of the co-intercalants [46]. Investigations of integrated systems within two-dimensional nanospace seem to have abated because of this difficulty despite their high potential. Recently, investigations were revived [23–38] in response to the current growing need to create integrated reaction systems such as solid-state artificial photosynthesis systems and dye-sensitized solar cells [29,36]. Although there are only limited reports, interesting integrated ET reaction systems have been constructed in the galleries of phyllosilicates [34,36] or suspensions of phyllosilicates and two different dyes [29]. Furthermore, challenging investigations [23,25,28,32] have been carried out on how the nano-level structure governs reactions. The time has come to embark on research that will reveal how the nano-level structure governs the reaction mechanisms and efficiencies within solid-state two-dimensional nanospace.

We have proposed [33] a unique and sound strategy wherein the key is to anchor one of the reaction substances covalently to the solid-state two-dimensional nanospace in order to overcome the problems of segregation and deintercalation. Our strategy is implemented as follows: first, one of the reaction substances, such as a functional dye or metal complex, is placed in the interlayer space of the phyllosilicate by covalently anchoring it to the interlayer surface of the phyllosilicate; thus, a hybrid consisting of reaction substance and phyllosilicate moieties is prepared [55–64]. This hybrid is referred to as the host hybrid and the substance is referred to as the host substance. Second, the integration of the target reaction substances is achieved by intercalation of another reaction substance (i.e., the guest substance) into the interlayer space of the host hybrid.

Coumarin and 3,3′-diethyloxacarbocyanine (DOC) are widely used as functional dyes and as spectral sensitizers for dye lasers and in photography in the liquid state [65–74]. Thermal *Z*/*E* isomerization, *E*/*Z* photoisomerization [66–68], and H- and J-aggregates [70] of DOC have been reported.

We previously reported preliminary results on the construction and interesting fluorescence behavior of coumarin/DOC systems, which suggested the occurrence of ET within the solid-state two-dimensional nanospace, using our proposed strategy as a *communication* intended for urgent publication [34]. However, the mole ratio of DOC to coumarin moiety ([DOC]/[Coum]) in that study was limited to a narrow range, and the mechanisms for the integration, interesting fluorescence behavior, and arrangements of the fluorophores were insufficiently addressed [34].

In our most recent investigation [35], we examined time-resolved photoluminescence (PL) and analyzed the PL transients in terms of a FRET model by taking into account the effect of radiative ET to reveal the mechanism for the interesting photoreaction between the coumarin moieties and DOC molecules in the integrated coumarin/DOC systems. This investigation revealed that the excited coumarin moiety transfers its excitation energy to DOC via at least two different paths, i.e., extremely fast FRET and radiative ET [35]. Further study is needed to explore the construction and characterization of these systems (including steady-state ultraviolet visible (UV–vis) absorption and fluorescence spectroscopy) and the arrangements of the fluorophores in the integrated coumarin/DOC systems with a wide range of [DOC]/[Coum].

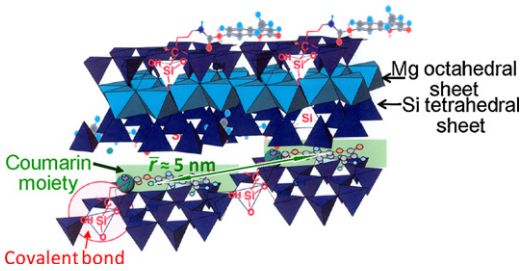

Scheme 1. Schematic view of host hybrid. $\bar{r}$ represents the average distance between the coumarin moieties.

The aims of this report are to demonstrate the construction of the integrated coumarin/DOC systems with a wide extended range of [DOC]/[Coum] and to reveal the steady-state fluorescence properties, the arrangements of the fluorophores (especially, the distances between the photoreactive substances), and the relevance of the fluorophore arrangement to the ET of the integrated coumarin/DOC systems. The construction of integrated systems with a wide range of [DOC]/[Coum] was successfully achieved by applying our strategy. The steady-state fluorescence spectroscopy results showed that both the coumarin moieties and DOC molecules fluoresce and that ET occurs from the coumarin moieties to DOC molecules in the integrated coumarin/DOC systems. Further, these emission intensities are relatively easily controlled by changing the concentration of DOC in the starting intercalation solutions. Unique fluorophore arrangement models are described by multiple D–A distances. Namely, some of the coumarin moieties are sufficiently close to the acceptor (DOC) to achieve FRET, while other coumarin moieties are too distant; all DOC molecules are close to a coumarin moiety. This unique fluorophore arrangement allows at least two types of simultaneous ET, i.e., FRET and radiative ET, in the same two-dimensional nanospace. Both the number of coumarin moieties close to acceptors and the extent of FRET increase as [DOC]/[Coum] increases.

2. Experimental

2.1. Materials

A coumarin/phyllosilicate host hybrid (Scheme 1) was synthesized by a reaction between 7-(3-triethoxysilylpropyl)-O-(4-methyl-coumarin)urethane ($C_{20}H_{29}NO_7Si$) and inorganic reagents (LiF, $Mg(OH)_2$ gel, and silica sol) [33,34,64] and not by the intercalation of organic molecules into the interlayers of phyllosilicate. The chemical formula of the host hybrid can be described as $(C_{14}H_{14}NO_4)_{0.01}(C_5H_{10}O_2N)_{0.2}Li_{0.16}(Li_{0.16}Mg_{2.84})Si_4O_{10}(OH)_2$ based on elemental analysis results. It was confirmed by X-ray diffraction (XRD), elemental analyses, infra-red spectra, and high-resolution solid-state ^{29}Si nuclear magnetic resonance spectroscopy that the synthesized coumarin/phyllosilicate hybrid consists of an Mg-phyllosilicate-analogue and coumarin moieties, and that the coumarin moieties (Scheme 2(a)) are anchored to and located between the layers of the inorganic Mg-phyllosilicate-analogue moieties [33,34,64].

3,3′-Diethyloxacarbocyanine iodide (DOCI) was purchased from Exciton, Inc. and used without further purification. Synthetic smectite (SWN) [75] was kindly donated by the Co-op Chemical Co., Ltd.

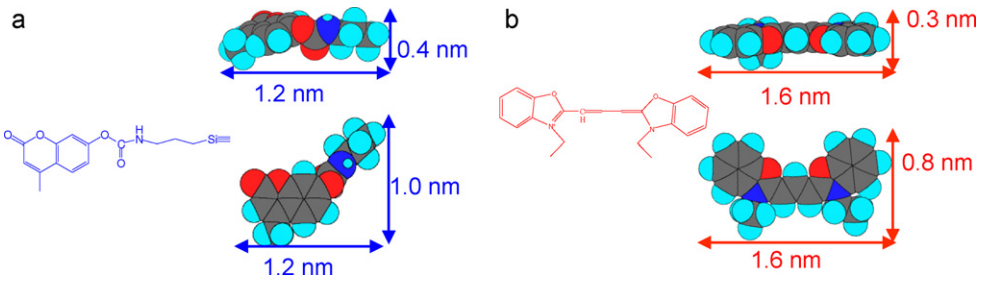

Scheme 2. Scheme of (a) coumarin moiety and (b) 3,3′-diethyloxacarbocyanine (DOC).

2.2. Preparation of integrated coumarin/DOC systems and DOC/smectite composites

The coumarin/phyllosilicate hybrid was utilized as the host hybrid for preparing the integrated coumarin/DOC systems. The DOC molecules were intercalated into the interlayer spaces in the host hybrid by adding 2–200 mL of aqueous solutions (2.00×10^{-6}, 2.00×10^{-5}, and 2.00×10^{-4} mol/L) of DOCI (3, 3′-diethyloxacarbocyanine iodide) to 2 mL of an aqueous dispersion of the host hybrid (the host hybrid/H_2O ratio was 0.020 g/mL). The ratios of DOC to the host hybrid (x) in the starting mixtures were 0.010, 0.10, 1.0, 10, and 100 mmol/100 g. For example, for $x = 0.10$, 2 mL of a DOCI aqueous solution with a concentration of 2.00×10^{-5} mol/L was used. 200 mL of a DOCI aqueous solution with a concentration of 2.00×10^{-4} mol/L was used for $x = 100$ (Supplementary data). After stirring the mixtures at room temperature for a week, yellowish precipitates were formed and then filtered, washed with water, and dried to yield the coumarin/DOC/phyllosilicate hybrids.

The DOC/smectite composites reference samples were prepared in a similar manner as the coumarin/DOC/phyllosilicate hybrids, except that SWN was used as the host instead of the host hybrid.

2.3. Characterization

Ultraviolet–visible (UV–vis) spectra were measured using a Jasco V-570 UV/VIS/NIR spectrophotometer. An integrating sphere was attached to the spectrophotometer for the powder samples. The coumarin/DOC/phyllosilicate hybrids with high DOC contents were diluted with barium sulfate ($BaSO_4$) because of strong absorptions by DOC. X-ray diffraction (XRD) measurements were performed at room temperature using CuKα radiation on a Rigaku Rint 2000S diffractometer equipped with a humidity/temperature-controlled chamber [76]. Fluorescence emission and excitation spectra were recorded with a Hitachi F-7000 fluorescence spectrophotometer. An integrating sphere was attached to the fluorescence spectrophotometer to measure the amount of fluorescence as a total integrated intensity of emission.

3. Results and discussion

3.1. Construction of integrated coumarin/DOC systems with a wide range of DOC/coumarin ratios within two-dimensional nanospace

Strong absorption peaks were observed at 480 and 458 nm in the UV–vis spectra of the DOCI aqueous solutions before the intercalation reactions (Fig. 1(a)). These absorptions are attributed to the DOC molecules [65–70]. Accordingly, only very weak absorptions due to DOC molecules were observed for the supernatants after the intercalation reactions (Fig. 1(b)). The UV–vis spectra also show several absorption peaks corresponding to the coumarin/DOC/phyllosilicate hybrids (Fig. 2). The absorption

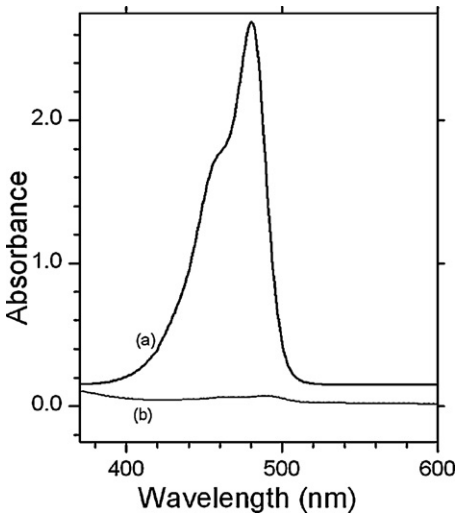

Fig. 1. UV–vis absorption spectra for (a) 2.00×10^{-5} mol/L DOCI aqueous solution and (b) supernatant after an intercalation reaction for $x = 0.10$.

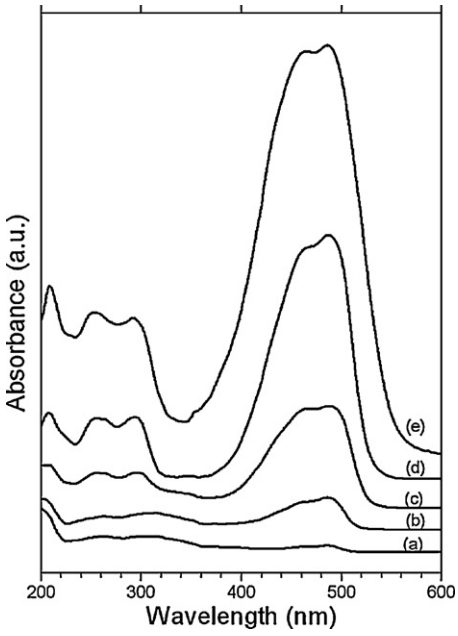

Fig. 2. UV–vis absorption spectra for the integrated coumarin/DOC systems prepared from the starting mixtures with x = (a) 0.010, (b) 0.10, (c) 1.0, (d) 10, and (e) 100 mmol/100 g. (The samples were diluted with $BaSO_4$ for $x = 10$ and 100. The spectra are enlarged by factors of 1.8 for $x = 10$ and 3.6 for $x = 100$. The factors were calculated by dividing the absorbance at 292 nm for the samples without dilution by the absorbance for the samples diluted with $BaSO_4$. The spectra without dilution are presented in Supplementary data.)

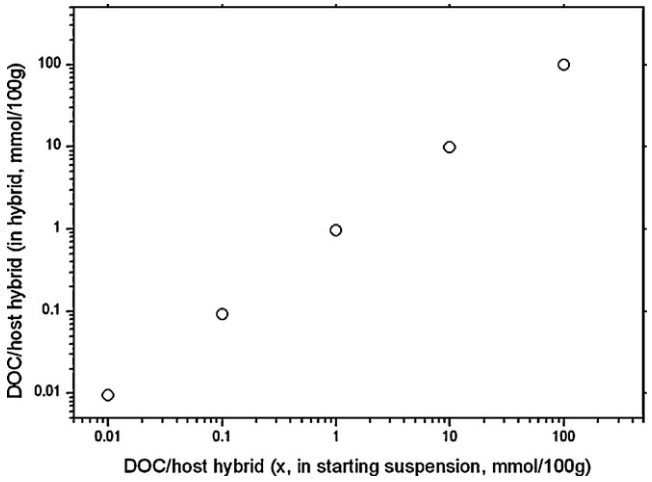

Fig. 3. Relationship between the content of DOC incorporated in the integrated coumarin/DOC systems (vertical axis) and the DOC/host hybrid ratios (x) in the starting mixtures (horizontal axis).

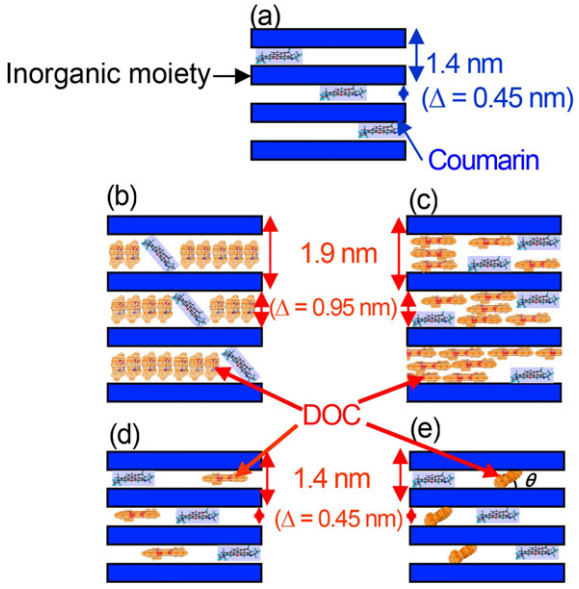

Scheme 3. Schematic representations of models for (a) host hybrid, (b and c) coumarin/DOC/phyllosilicate hybrid with $x = 100$, and (d and e) with $x = 0.010$–10.

peaks were observed around 488, 466, 293, 255, and 205 nm. These absorptions are attributed to DOC [65–70]. The absorption peaks increase in intensity in the UV–vis spectra of the coumarin/DOC/phyllosilicate hybrids as the concentration of DOC (x) in the starting mixtures is raised. The strong peak at around 466 nm is attributed to absorption by the E-isomer resulting in isomerization to the Z-isomer as well as an excitation [66–68,77–80]. Another strong absorption peak at around 488 nm is attributed to the Z-isomer of the DOC molecules [66–68]. Thermal Z/E isomerization and E/Z photoisomerization reactions are well known for DOC molecules [68]. It has been reported that the E-isomer fluoresces whereas the Z-isomer does not fluoresce [66–68]. It has also been reported that H-aggregates (sandwich aggregates) are not fluorescent while J-aggregates (head-to-tail aggregates) are, and that absorption due to the J- and H-aggregates has been observed at around 560 nm and 455 nm, respectively [70]. No peak or shoulder was observed around these wavelengths in the UV–vis spectra of the coumarin/DOC/phyllosilicate hybrids (Fig. 2). However, a small absorption due to J-aggregates could be overlapped with the longer wavelength side of the broad absorption around 488 nm. Also, the absorption due to H-aggregates may be overlapped with the broad absorption around 466 nm for the coumarin/DOC/phyllosilicate hybrids when $x = 100$ (Fig. 2(e)). H-aggregates are not formed in the coumarin/DOC/phyllosilicate hybrids when $x = 0.010$–10 because the clearance spaces between the phyllosilicate moieties do not allow for the formation of H-aggregates, as described below. The absorption peaks in the short wavelength range (200–300 nm) can be described as a characteristic of the condensed ring [71]. Thus, the UV–vis spectra show that DOC is incorporated into the coumarin/DOC/phyllosilicate hybrids over a wide content range. A broad absorption peak is also observed at around 330 nm. This absorption is due to the coumarin moiety. This absorption is observed for samples with low x, as shown in Fig. 2(a) and (b) [81], but becomes difficult to observe as x increases. This can be attributed to the overlap with the absorption by DOC. It is well known that phyllosilicate layers are almost transparent in visible light. They are not completely transparent in the UV region, but they do not show a characteristic peak. Fig. 3 shows the dependence of the ratio of incorporated DOC molecules to the hybrid on x. The ratio is calculated from the change in the concentration of the DOC aqueous solutions before and after the intercalation reactions. As x increases, the ratio of the incorporated DOC to the host hybrid increases from 0.0095 mmol/100 g for $x = 0.010$ to 100 mmol/100 g for $x = 100$. These ratios correspond to the extensive range of [DOC]/[Coum] of 0.004 ($x = 0.010$)–40 mol/mol ($x = 100$). Surprisingly, the ratio of incorporated DOC is not saturated in the wide range studied here ($0.010 \leq x \leq 100$ mmol/100 g).

The interlayer distance of the host hybrid is about 1.4 nm [33,34,64]. Therefore, since the thickness of an inorganic layer is approximately 0.95 nm, the clearance space between the layers is about 0.45 nm [82]. Scheme 2(a) schematically represents a model of the energy minimized structure calculated [83] for the coumarin moiety, which is estimated to be about 0.4 nm thick. The coumarin moiety is considered to be aligned nearly parallel to the Si–O–Si surface of the inorganic layers in the host hybrid (Scheme 3(a)) [33,34,64]. Fig. 4 shows the XRD patterns of the coumarin/DOC/phyllosilicate hybrids. The XRD pattern in Fig. 4(e) shows that the interlayer distance is approximately 1.9 nm for the coumarin/DOC/phyllosilicate hybrid with $x = 100$. This increase in the interlayer distance shows explicitly that the guest is incorporated into the interlayers of the host hybrid, i.e., an integrated coumarin/DOC system is constructed within the solid-state two-dimensional nanospace between the inorganic layers. The thickness is about 0.3 nm and the width is about 0.8 nm for the DOC molecule, as shown in Scheme 2(b). The clearance space between the inorganic layers is evaluated to be about 0.95 nm for the integrated coumarin/DOC system with $x = 100$. For the integrated coumarin/DOC system with a large clearance space (0.95 nm), many models can be proposed. One example is shown in Scheme 3(b) and features the DOC molecules aligned perpendicular to the Si–O–Si surface of the inorganic moiety. Another model can also be proposed, as shown in Scheme 3(c). In this model, the DOC molecules are aligned nearly parallel to the silicate surface and stacked with three layers of DOC molecules. The XRD patterns in Fig. 4(a–d) show that the interlayer distances are about 1.4 nm for the coumarin/DOC/phyllosilicate hybrids with $x = 0.010$–10, i.e., the interlayer distances are the same as that of the host hybrid. The clearance spaces are about 0.45 nm for the coumarin/DOC/phyllosilicate hybrids with $x = 0.010$–10. Two models can be proposed for these coumarin/DOC/phyllosilicate hybrids, as shown in Scheme 3(d) and (e). In the model shown in Scheme 3(d), the DOC molecules are aligned nearly parallel to the inorganic sheet. In the model shown in Scheme 3(e), the DOC molecules are oriented with a tilting angle (θ) of approximately 30° with respect to the silicate surface.

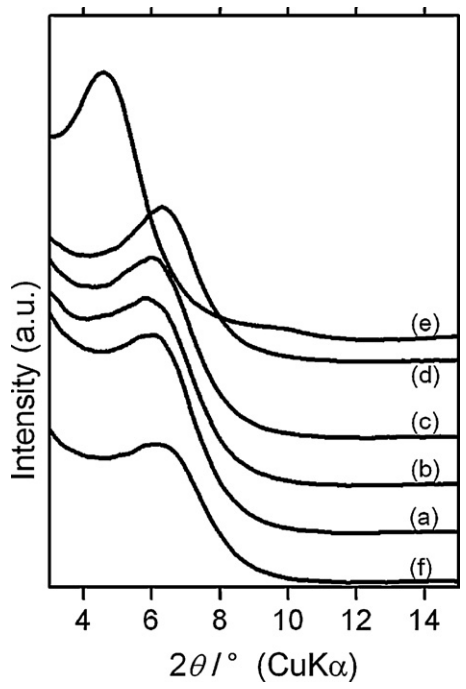

Fig. 4. XRD patterns for the integrated coumarin/DOC systems prepared from the starting mixtures with x = (a) 0.010, (b) 0.10, (c) 1.0, (d) 10, and (e) 100 mmol/100 g and (f) the host hybrid as a reference.

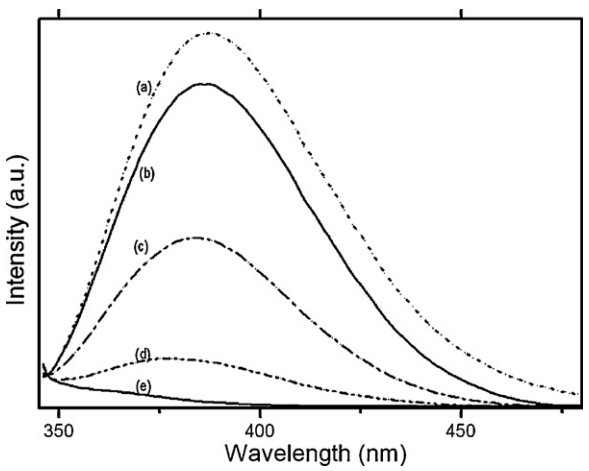

Fig. 5. Emission spectra for the integrated coumarin/DOC systems with x = (a) 0.010, (b) 0.10, (c) 1.0, (d) 10, and (e) 100 mmol/100 g, λ_{ex} = 320 nm. (Spectra were normalized as follows: each spectrum is enlarged (reduced) by the emission intensity at 347 nm and baseline subtracted.)

The clearance space between the layers allows about 66 mmol of DOC molecules per 100 g of the host hybrid with a 1.4 nm interlayer distance based on the sizes shown in Scheme 2(b). When DOC molecules are intercalated into the interlayer spaces in excess of this threshold value, the space between the inorganic layers should expand, which does, in fact, occur, as shown in Fig. 4. The incorporated DOC is 100 mmol/100 g for the integrated coumarin/DOC systems with x = 100, and 9.9 mmol/100 g for x = 10, as shown in Fig. 3.

The chemical formula for the host hybrid can be described as $(C_{14}H_{14}NO_4)_{0.01}(C_5H_{10}O_2N)_{0.2}Li_{0.16}(Li_{0.16}Mg_{2.84})Si_4O_{10}(OH)_2$ based on elemental analysis results. The intercalation of the dye into the host hybrid can be carried out by an ion exchange reaction with Li ions up to 0.16 per formula, i.e., up to 40 mmol/100 g. The incorporated DOC is 0.009–9.9 mmol/100 g for the coumarin/DOC/phyllosilicate hybrids with x = 0.010–10. Therefore, the DOC cation can be loaded into the interlayer of the host hybrid by the ion exchange reaction. However, the incorporated DOC is 100 mmol/100 g for the coumarin/DOC/phyllosilicate hybrid with x = 100. Therefore, at least 60% of the incorporated DOC is loaded into the interlayer of the host hybrid by reactions other than the ion exchange reaction. The interlayer of the host hybrid is hydrophobic due to the coumarin moieties and the incorporated DOC. It can be speculated that the cyanine molecules are stable in the hydrophobic interlayer of the host hybrid rather than in the aqueous solution during the intercalation reaction. Therefore, this would allow the cyanine molecules to penetrate into the interlayers of the host hybrid in such a large amount. This model for the intercalation reaction demonstrates that this strategy has the potential to be applied to the construction of new integrated systems with neutral or anionic functional guests.

DOC can be adsorbed on the external surface as well as in the interlayers of the host hybrid [84]. Assuming that the guest adsorbs initially on the external surface of the layered host materials and the guest then intercalates into the interlayers after the external surface is completely covered, all of the DOC could be adsorbed only on the external surface of the host hybrid when x = 0.010–1.0. For the coumarin/DOC/phyllosilicate hybrids with x = 10 and 100, 68% and 98% of the adsorbed DOC is located within the interlayers of the host hybrid, respectively. We will discuss this further and show that the DOC molecules are dominantly adsorbed on the interlayers in Section 3.3.

We achieved the construction of integrated coumarin/DOC systems with a wide range of mole ratios ([DOC]/[Coum] of 0.004–40 mol/mol) within the solid-state two-dimensional nanospace. The [DOC]/[Coum] can be accurately controlled by changing the concentration of DOC in the intercalation solutions because the coumarin moieties are anchored to the inorganic layers and therefore, the amount of incorporated coumarin does not change.

3.2. Fluorescence behavior and energy transfer in integrated coumarin/DOC systems

An emission is observed at around 385 nm when the integrated coumarin/DOC systems within the solid-state two-dimensional nanospace are excited at the absorption maxima of the neutral coumarin, i.e., 320 nm, as shown in Fig. 5. This emission is attributed to the neutral form of the coumarin moiety [64,72]. The emission intensity decreases as x increases. The decrease is correlated with the intercalation of DOC, as described in detail in the next section.

Emissions are observed around 520 nm when the integrated coumarin/DOC systems are excited at 480 nm, as shown in Fig. 6. These emissions are attributed to DOC [65–70]. Both the coumarin moiety and DOC can fluoresce even in the integrated coumarin/DOC systems, resulting in the formation of a solid-state luminous material with a wide fluorescence wavelength of 350–600 nm. The emissions become intense as x increases in the low content range (x = 0.010–0.10 mmol/100 g). In contrast, the emission intensities decrease as x increases in the relatively higher content range (x = 0.10–100), especially when $x \geq 10$. The enhancement in the low content range is caused by the increase of the fluorophore content. The decrease in the relatively higher content range could be attributed to quenching including ET to other DOC molecules and/or aggregates, electron transfer, etc. The quenching could also be related to clustering (see the following section).

The emission from DOC shifts to longer wavelengths depending on the value of x. Several mechanisms can be proposed for the red

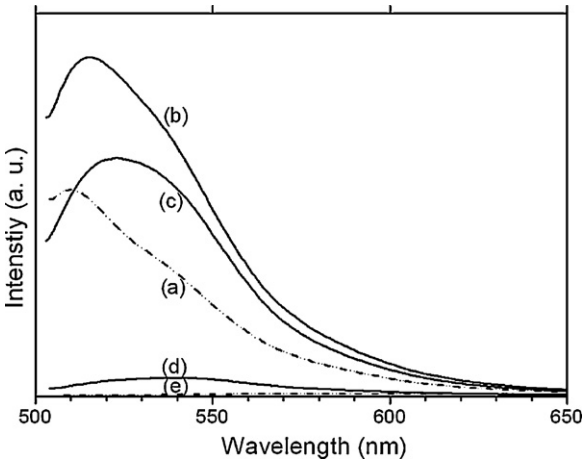

Fig. 6. Emission spectra for the integrated coumarin/DOC systems with x = (a) 0.010, (b) 0.10, (c) 1.0, (d) 10, and (e) 100 mmol/100 g, λ_{ex} = 480 nm.

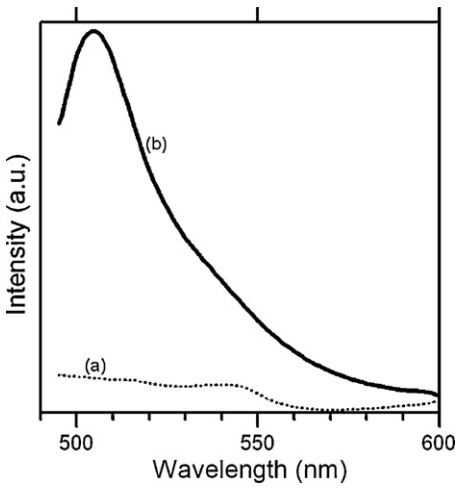

Fig. 8. Emission spectra for the DOC/smectite hybrid, λ_{ex} = (a) 320 (dashed) and (b) 480 nm (solid).

shift: (1) the homo-reabsorption effect by DOC molecules or aggregates [85], (2) clustering, (3) the formation of a charge-transfer state with an excited state at a lower energy level [86], and (4) interaction with the environment, especially the Si–OH groups of the inorganic moieties [64,73], etc. The homo-reabsorption effect, the formation of the clusters of fluorophores, and/or the formation of a charge-transfer state are more likely because these should become more significant as the DOC content increases. The red-shift will be discussed in more detail elsewhere.

Surprisingly, emissions from DOC are observed around 520 nm even when the integrated coumarin/DOC systems are excited at 320 nm, as shown in Fig. 7. The emission intensity from DOC increases as x increases in the relatively low content range (x = 0.010–1.0). The emission intensity from the coumarin moieties decreases as x increases. In particular, the emission from the coumarin moiety decreases considerably at x = 10 ([DOC]/[Coum] = 4) and is hardly observed at x = 100 ([DOC]/[Coum] = 40). DOC hardly fluoresces in the DOC/smectite composites and DOC aqueous solution when excited at 320 nm, as shown in Fig. 8. The fluorescence emissions from DOC are observed around 510 nm for the DOC/smectite composites (Fig. 8(b)) and the DOC aqueous solutions when excited at the absorption maxima of DOC. Two mechanisms can be proposed as follows:

(1) The first one is non-radiative ET (e.g., FRET) from the excited coumarin moieties (donors) to the DOC molecules (acceptors), which results in the observed emission from the acceptor (DOC). FRET results from long-range dipole–dipole interactions between the donor and acceptor (Förster model) [51,52].
(2) The second proposed mechanism is radiative ET due to emission from the coumarin moieties and reabsorption of the photon by the DOC molecules. This would also result in the observed emission from DOC.

The absorption spectra of DOC in the integrated coumarin/DOC systems overlap with the emission spectrum of the coumarin moieties in the host hybrid, as shown in Fig. 9. This spectral overlap indicates that FRET can occur from the coumarin moiety to DOC in the integrated coumarin/DOC systems [8] since FRET can occur in systems where the absorption spectrum of the acceptor overlaps with the emission spectrum of the donor when the D–A distance is comparable to or less than R_0 [51]. However, radiative ET can also occur in systems with spectral overlap.

The amount of fluorescence from the donor should be smaller for systems in which FRET occurs than for systems without the

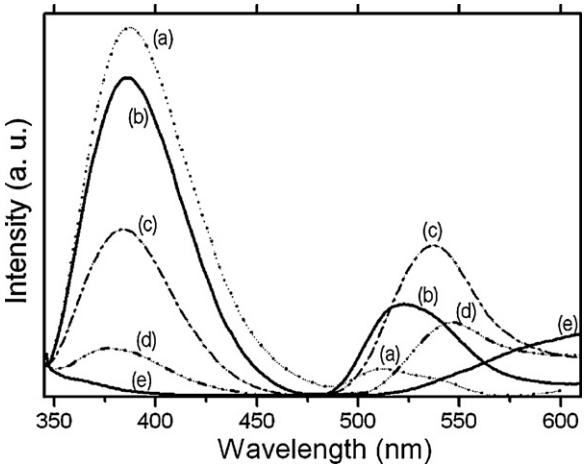

Fig. 7. Emission spectra for the integrated coumarin/DOC systems with x = (a) 0.010, (b) 0.10, (c)1.0, (d)10, and (e) 100 mmol/100 g, λ_{ex} = 320 nm. (Each spectrum is enlarged (reduced) by the emission intensity at 347 nm and baseline subtracted.)

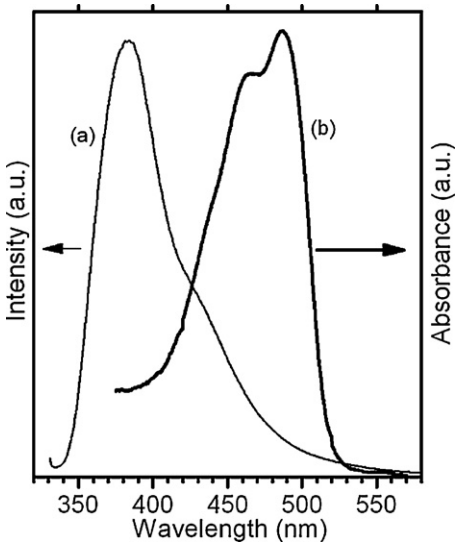

Fig. 9. (a) Emission spectrum for the host hybrid, λ_{ex} = 320 nm and (b) UV–vis absorption spectrum for the integrated coumarin/DOC system with x = 0.10.

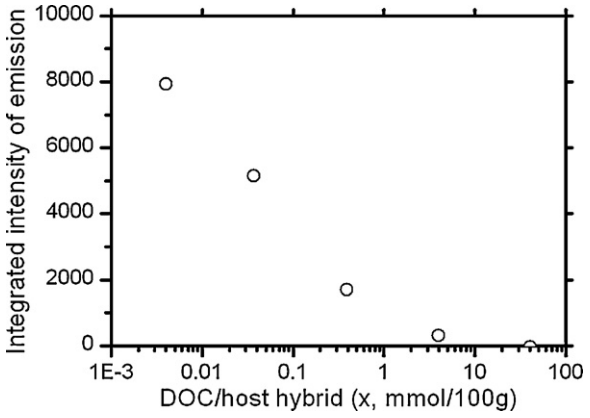

Fig. 10. Dependence of the integrated emission intensity at around 385 nm on x (the DOC/host hybrid ratios in the starting mixtures). The integrated coumarin/DOC systems were excited at 320 nm. The emission spectra were measured using a fluorescence spectrophotometer equipped with an integrating sphere attachment.

acceptor present and should therefore decrease as the ratio of acceptors to donors increases. Fig. 10 shows the experimental data for the integrated intensity of the emission from the coumarin moiety in the integrated coumarin/DOC systems with various x values. The integrated intensity of the emission from the coumarin moiety decreases as x increases. Furthermore, the integrated intensities are smaller for the integrated coumarin/DOC systems than for the coumarin moieties in the host hybrid, i.e., the system without the acceptor. The integrated intensity for the integrated coumarin/DOC system with $x = 0.010$ is about ¾ of the integrated intensity for the host hybrid. However, the integrated intensity of the emission should also be smaller if radiative ET occurs.

The experimental results indicate the occurrence of ET from the coumarin moieties to the DOC molecules, as described above. However, it is difficult to distinguish via which path, i.e., FRET or radiative ET, the ET occurs. FRET should be dominant if the distance between the coumarin moieties and DOC (D–A distance) is comparable to or less than R_0 for the integrated coumarin/DOC systems. This is because FRET occurs much faster than radiative ET in systems where the D–A distance is less than or equal to R_0. When the coumarin moiety is located far from the DOC molecules, radiative ET would primarily occur. The integrated coumarin/DOC systems with a wide range of [DOC]/[Coum] provide wide range of ET and various arrangements of fluorophores. This wealth of information enables discussions on the nano-level structure and relevance of the nano-level structure to the ET mechanism, as we will discuss in the next section.

The integrated coumarin/DOC systems are attractive materials for certain applications. The integrated coumarin/DOC systems emit over a wide range of wavelengths, from 350 to 600 nm, in response to only one excitation at 320 nm; therefore, the emission in a wide wavelength range does not need several excitations at different wavelengths, as shown in Fig. 7. Furthermore, the emission intensities vary extensively over the wide range of [DOC]/[Coum] (Fig. 10) and are relatively easily controlled by changing the concentration of DOC in the starting intercalation solutions. It is demonstrated that the construction of the integrated coumarin/DOC systems with extended [DOC]/[Coum] values provide fluorescent materials with user-defined fluorescence intensities.

3.3. Arrangements of fluorophores and energy transfer mechanisms in the integrated coumarin/DOC systems

Each of the coumarin moieties occupies a mean area of 26 nm^2 in the host hybrid (Supplementary data). Thus, the mean distance

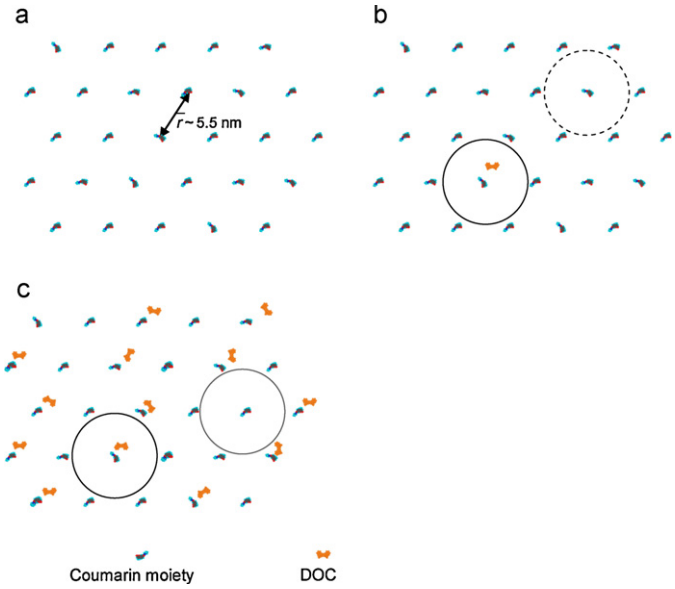

Scheme 4. Schematic representations of proposed fluorophore arrangement models for (a) host hybrid and the integrated coumarin/DOC systems with (b) $x \leq 0.10$ and (c) $x = 1.0$. $\bar{r}$ represents the average distance between the coumarin moieties. The radius of each circle is equal to the Förster distance for the integrated coumarin/DOC systems.

between neighboring coumarin moieties is estimated to be 5.5 nm. Scheme 4(a) illustrates the arrangement of coumarin moieties before intercalating the DOC molecules. When the DOC molecules are intercalated, the coumarin moieties do not migrate because they are anchored to the inorganic moiety by a covalent bond. Consequently, every DOC molecule is within R_0 of a coumarin moiety regardless of the [DOC]/[Coum] and DOC position (Scheme 4(b) and (c)). A characteristic scale is known as the Förster distance (R_0) [1,2,5,10,12–15,23,51,52], which was estimated to be 4.2 nm for the integrated coumarin/DOC systems [87].

Scheme 4(b) shows the expected arrangement of fluorophores in the integrated system with a low [DOC]/[Coum] ($x \leq 0.1$). We found that many of the coumarin moieties are far away from any DOC molecule (dotted circle), although some coumarin moieties are close to DOC molecules (solid circle) within the same two-dimensional nanospace. In this manner, a unique fluorophore arrangement is achieved. The most important factor in the construction of a unique fluorophore arrangement is the anchoring of the coumarin moiety to the inorganic moiety through the covalent bond. It is not sufficient here to describe the fluorophore arrangements by the mean D–A distance estimated simply from the total density of the fluorophores per unit area. It should be noted that the rate of energy transfer (k_T) for the integrated coumarin/DOC systems is not given by $k_T = \frac{1}{\tau_D}\left(\frac{R_0}{r}\right)^6$, which is only applicable to isolated donor–acceptor pairs. For energy transfer systems with multiple D–A distances within a two-dimensional surface, the intensity decay of the donor is given by integrating the intensity decay for the distribution of the multiple D–A distances [88].

An increase in [DOC]/[Coum] leads to an increase in the number of coumarin moieties that are within a radius of R_0 from a DOC molecule, as illustrated in Scheme 4(c) ($x = 1.0$) and Scheme S2 (a tentative model for $x = 10$). The proportions of such coumarin moieties, which contribute to FRET, are estimated at about 2, 15, and 70% for $x = 0.010$, 0.10, and 1.0, respectively, while all DOC molecules are close to a coumarin moiety. For $x = 100$, many DOC molecules surround each coumarin moiety, as shown in Scheme 3.

In general, FRET becomes the dominant ET path over radiative ET as the D–A distance becomes shorter. When the donor is excited

by incident light in cases with a D–A distance comparable to or less than R_0, FRET can occur from many of the excited donors to the adjacent acceptors. In contrast, when the D–A distance is significantly longer than R_0, the excited donor itself fluoresces. Many of the photons radiated from the excited donors are emitted out of the systems, while some of the photons are absorbed by the acceptors. As a result, the acceptor is excited via radiative ET. Indeed FRET occurs even in integrated systems with D–A distances longer than R_0. However, FRET becomes slower than the emission from the donor and the excited donors transfer energy mainly via radiative ET in systems with D–A distance greater than R_0.

Almost all of the excited coumarin moieties would transfer their excited energy to DOC molecules via FRET in the proposed fluorophore arrangement models of the integrated coumarin/DOC systems with $x = 10$ and 100 because the D–A distance is shorter than R_0 for every coumarin moiety. In the proposed fluorophore arrangement models for $x \leq 1.0$, the excited coumarin moieties would undergo ET via at least two different paths: (1) FRET from the excited coumarin moieties close to DOC molecules (D–A distance $\leq R_0$ for the coumarin moiety) and (2) radiative ET from the excited coumarin moieties far from any DOC molecules (D–A distance is significantly longer than R_0 for the coumarin moiety).

Furthermore, the extent of FRET is considered to vary with [DOC]/[Coum] because the number of coumarin moieties close to DOC molecules increases as [DOC]/[Coum] increases. Therefore, the extent of FRET can be relatively easily controlled by changing the concentration of DOC in the intercalation solutions.

ET can also occur via the Dexter mechanism in systems such as the integrated coumarin/DOC system with $x = 100$. It is well known that Dexter-type (electron exchange process) ET can occur in a system where the donor and acceptor are in contact with each other, i.e., the electron orbitals of the donor and acceptor overlap. Of course, a number of the excited fluorophores also return to the ground state by radiationless deactivation. It is well known that an ET can occur across two-dimensional surfaces such as layered double hydroxide layers by the Förster mechanism [10,19]. However, the nano-level structure in a two-dimensional nanospace is sufficient for the practical discussion of how the mechanism and extent of ET are governed by the nano-level structure, i.e., the distances and relative disposition between the fluorophores in the integrated coumarin/DOC systems. This is because the shortest D–A distance within the two-dimensional nanospace is estimated to be shorter than the shortest D–A distance across the inorganic sheet.

We will discuss here the D–A distance between the coumarin moieties and DOC molecules in more detail (Scheme S3). During intercalation, the DOC molecules settle where the intermolecular potential energy is minimized with regard to the coumarin moiety. Such a condition is met when the intermolecular distance is slightly longer than the closest approach between the molecules. We also note that, because the Si–OH group is localized around the coumarin moiety in the inorganic surface (Supplementary data), cationic DOC molecules are more drawn to the coumarin moieties. The resultant short intermolecular distance allows FRET to occur in very short time scales. In fact, our study of time-resolved PL confirmed an ultra-fast FRET process occurring on the scale of a few picoseconds in addition to the radiative ET path [35].

The fluorophores may cluster in the integrated coumarin/DOC system with $x = 10$, as shown in Scheme 5, because the DOC content is high and the DOC molecules are close to each other (Supplementary data, Scheme S2). If the fluorophore arrangement can be represented by the tentative model without clusters, as shown in Scheme S2, almost all of the excited coumarin moieties can transfer their excited energy to the surrounding DOC molecules via FRET and therefore emission from the coumarin moieties should be barely observable for the integrated coumarin/DOC system

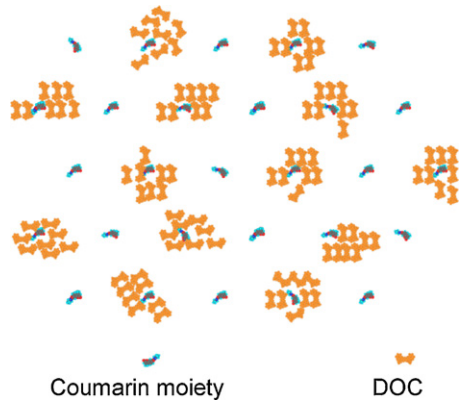

Scheme 5. Schematic view of proposed model of nano-level structure for the integrated coumarin/DOC systems with $x = 10$.

with $x = 10$. In this manner, the tentative fluorophore arrangement model without the cluster (Scheme S2) conflicts with the experimental results of the steady-state fluorescence measurements. However, the proposed fluorophore arrangement model (Scheme 5) with the clusters is consistent with the experimental results. Indeed, even some of the coumarin moieties excluded from the clusters can transfer excited energy to the DOC molecules via FRET, but the extent of FRET will not be high. Furthermore, the results of the time-resolved PL in our previous report [35] are consistent with the fluorophore arrangement model with the clusters (Scheme 5) for the integrated coumarin/DOC system with $x = 10$ and the fluorophore arrangement model without clusters (Scheme 4(c)) for $x = 1.0$. Thus, as x increases, the D–A distance tends to shorten for the coumarin moieties (whereas the D–A distance $< R_0$ for all DOC molecules, even at low x) and the fluorophores become denser, resulting in stronger intermolecular forces, e.g., van der Waals forces, and the ultimate formation of fluorophore clusters. Takagi et al. proposed a partially clustered nano-level structure but without aggregation for porphyrins in interesting clay-porphyrin complexes even with a low concentration of porphyrins (0.4% vs. cationic exchange capacity (CEC)) [23]. CEC was reported to be 99.7 meq/100 g for the clay used in their investigation [23]. Cyanine derivatives are well known to aggregate well even at very low concentrations [89–91]. The fluorophores are considered to form clusters in the integrated coumarin/DOC systems until the [DOC]/[Coum] becomes high ($x = 10$), as described above. This may be because the coumarin moieties are anchored apart from each other and the interactions between the coumarin moieties and DOC molecules could be stronger than those among the DOC molecules.

Assuming that the DOC molecules adsorb preferentially on the external surface rather than in the interlayer of the host hybrid, FRET would rarely occur in the systems with $x \leq 1.0$. This is because, based on this assumption, all the DOC molecules are assumed to adsorb only on the external surface for coumarin/DOC/phyllosilicate hybrids with $x \leq 1.0$, as described in Section 3.1. The occurrence of ultra-fast FRET [35] demonstrates that the DOC molecules are intercalated into the interlayers even in the case of the low DOC content ($x \leq 1.0$).

4. Conclusion

The integrated coumarin/DOC systems were constructed with an extended [DOC]/[Coum] range of 0.004–40 mol/mol in the solid-state two-dimensional nanoscale space between inorganic layers using the strategy proposed by us. This is achieved by utilizing the coumarin/phyllosilicate hybrid in which the coumarin moieties are covalently anchored to the phyllosilicate moieties. DOC molecules are loaded in excess of the limit by ion exchange reaction,

which demonstrates the potential to deploy this strategy to various systems even with neutral guest species. This successful construction provides a series of systems with a wide extent of FRET and various nano-level structures. The [DOC]/[Coum], fluorescence intensities, and the extent of FRET can be controlled relatively easily by changing the concentration of DOC in the starting intercalation solutions. The proposed nano-level structures are described with the coumarin moieties both close to and far from the DOC molecules in the same solid-state two-dimensional nanospace, while every DOC molecule is close to a coumarin moiety. The integrated coumarin/DOC systems are also useful as attractive fluorescent materials with a wide range of emission wavelengths from 350 to 600 nm by only one excitation at 320 nm and user-defined fluorescence intensities. The sound construction strategy and the knowledge of how the nano-level structures govern the mechanisms and extents of the ET reactions reported herein can be applied to provide new integrated systems. These systems will be constructed with suitable nano-level structures for target reactions such as ET and electron transfer reactions. One of the most important goals would be the realization of integrated reaction systems with tailored functions, e.g., artificial photosynthesis systems, dye-sensitized solar cells, etc.

Acknowledgements

We are grateful to Dr. Toshihiro Ando, Dr. Shuichi Shimomura, and Dr. Hideo Hashizume, NIMS, for their helpful discussions, Ms. Tomoko Kuwabara, NIMS, for her support, and Co-op Chemical Co. Ltd. for kindly donating their SWN (synthetic smectite). This work was partially supported by a Grant-in-Aid for Scientific Research (C) (21550196) from the Japan Society for the Promotion of Science.

Appendix A. Supplementary data

Supplementary data associated with this article can be found, in the online version, at doi:10.1016/j.jphotochem.2011.10.009.

References

[1] N. Mizoshita, T. Tani, S. Inagaki, Syntheses, properties and applications of periodic mesoporous organosilicas prepared from bridged organosilane precursors, Chem. Soc. Rev. 40 (2011) 789–800.
[2] S. Inagaki, O. Ohtani, Y. Goto, K. Okamoto, M. Ikai, K. Yamanaka, T. Tani, T. Okada, Light harvesting by a periodic mesoporous organosilica chromophore, Angew. Chem. Int. Ed. 48 (2009) 4042–4046.
[3] T. Tani, N. Mizoshita, S. Inagaki, Luminescent periodic mesoporous organosilicas, J. Mater. Chem. 19 (2009) 4451–4456.
[4] S. Angelos, E. Johansson, J.F. Stoddart, J.I. Zink, Mesostructured silica supports for functional materials and molecular machines, Adv. Funct. Mater. 17 (2007) 2261–2271.
[5] P.N. Minoofar, B.S. Dunn, J.I. Zink, Multiply doped nanostructured silicate sol–gel thin films: spatial segregation of dopants, energy transfer, and distance measurements, J. Am. Chem. Soc. 127 (2005) 2656–2665.
[6] H. Furukawa, N. Inoue, T. Watanabe, K. Kuroda, Energy transfer between chlorophyll derivatives in silica mesostructured films and photocurrent generation, Langmuir 21 (2005) 3992–3997.
[7] S. Murata, H. Furukawa, K. Kuroda, Effective inclusion of chlorophyllous pigments into mesoporous silica modified with α,ω-diols, Chem. Mater. 13 (2001) 2722.
[8] S. Kim, T.Y. Ohulchanskyy, H.E. Pudavar, R.K. Pandey, P.N. Prasad, Organically modified silica nanoparticles co-encapsulating photosensitizing drug and aggregation-enhanced two-photon absorbing fluorescent dye aggregates for two-photon photodynamic therapy, J. Am. Chem. Soc. 129 (2007) 2669–2675.
[9] T. Ban, D. Brühwiler, G. Calzaferri, Selective modification of the channel entrances of zeolite L with triethoxysilylated coumarin, J. Phys. Chem. B 108 (2004) 16348–16352.
[10] T. Yui, T. Kameyama, T. Sasaki, T. Torimoto, K. Takagi, Pyrene-to-porphyrin excited singlet energy transfer in LBL-deposited LDH nanosheets, J. Porphyrins Phthalocyanines 11 (2007) 428–433.
[11] B.K. Fung, L. Stryer, Surface density determination in membranes by fluorescence energy transfer, Biochemistry 17 (24) (1978) 5241–5248.
[12] J. Hill, Y. Heriot, O. Worsfold, T.H. Richardson, A.M. Fox, Controlled Förster energy transfer in emissive polymer Langmuir–Blodgett structures, Phys. Rev. B 69 (2004) 041303–41311.
[13] B. Richter, S. Kirstein, Excitation energy transfer between molecular thin layers of poly(phenylene vinylene) and dye labeled poly(allylamine) in layer-by-layer self-assembled films, J. Chem. Phys. 111 (1999) 5191–5200.
[14] I. Yamazaki, M. Yamaguchi, N. Okada, S. Akimoto, T. Yamazaki, N. Ohta, Non-equilibrium excitation energy transfer in sequentially stacking molecular systems, J. Lumin. 72–74 (1997) 71–74.
[15] E.R. Kleinfeld, G.S. Ferguson, Stepwise formation of multilayered nanostructural films from macromolecular precursors, Science 265 (1994) 370–373.
[16] T. Yatsue, T. Miyashita, Electron-transfer quenching accompanied by highly efficient energy migration in polymer Langmuir–Blodgett films, J. Phys. Chem. 99 (1995) 16047–16051.
[17] Md. Mahadozamen, T. Nakabayashi, S. Kang, H. Imahori, N. Ohta, External electric field effects on absorption and fluorescence spectra of a fullerene derivative and its mixture with zinc-tetraphenylporphyrin doped in a PMMA film, J. Phys. Chem. B 110 (2006) 20354–20361.
[18] Y. Yonezawa, T. Hayashi, Excitation energy transfer between J-aggregates of cyanine dyes arranged in a layer structure, J. Lumin. 47 (1990) 49–58.
[19] D.R. Haynes, A. Tokmakoff, S.M. George, Distance dependence of electronic energy transfer between donor and acceptors: p-terphenyl and 9,10-diphenylanthracene, J. Chem. Phys. 100 (3) (1994) 1968–1980.
[20] D.M. Kaschak, J.T. Lean, C.C. Waraksa, G.B. Saupe, H. Usami, T.E. Mallouk, Photoinduced energy and electron transfer reactions in lamellar polyanion/polycation thin films: toward an inorganic "leaf", J. Am. Chem. Soc. 121 (1999) 3435–3445.
[21] P.G. Hoerts, T.E. Mallouk, Light-to-chemical energy conversion in lamellar solids and thin films, Inorg. Chem. 44 (2005) 6828–6840.
[22] S. Peralta, J.-L. Habib-Jiwan, A.M. Jonas, Ordered polyelectrolyte multilayers: unidirectional FRET cascade in nanocompartmentalized polyelectrolyte multilayers, ChemPhysChem 10 (2009) 137–143.
[23] S. Takagi, M. Eguchi, H. Inoue, Energy transfer reaction of cationic porphyrin complexes on the clay surface: effect of sample preparation method, Res. Chem. Intermed. 33 (2007) 177–189.
[24] S. Takagi, M. Eguchi, D.A. Tryk, H. Inoue, Porphyrin photochemistry in inorganic/organic hybrid materials: clays, layered semiconductors, nanotubes, and mesoporous materials, J. Photochem. Photobiol. C: Photochem. Rev. 7 (2006) 104–126.
[25] S. Takagi, M. Eguchi, D.A. Tryk, H. Inoue, Light-harvesting energy transfer and subsequent electron transfer of cationic porphyrin complexes on clay surfaces, Langmuir 22 (2006) 1406–1408.
[26] S. Takagi, Kagaku to Kogyo 58 (2005) 121–124.
[27] S. Takagi, D.A. Tryk, H. Inoue, Photochemical energy transfer of cationic porphyrin complexes on clay surface, J. Phys. Chem. B 106 (2002) 5455–5460.
[28] S. Takagi, T. Shimada, T. Yui, H. Inoue, High density adsorption of porphyrins onto clay layer without aggregation: characterization of smectite-cationic porphyrin complex, Chem. Lett. 30 (2001) 128–129.
[29] A. Czímerová, N. Iyi, J. Bujdák, Fluorescence resonance energy transfer between two cationic laser dyes in presence of the series of reduced-charge montmorillonites: effect of the layer charge, J. Colloid Interface Sci. 320 (2008) 140–151.
[30] A. Czímerová, N. Iyi, J. Bujdák, Fluorescence resonance energy transfer between laser dyes in saponite dispersions, J. Photochem. Photobiol. A 187 (2007) 160–166.
[31] J. Bujdák, J.D. Chorvát, N. Iyi, Resonance energy transfer between rhodamine molecules adsorbed on layered silicate particles, J. Phys. Chem. C 114 (2010) 1246–1252.
[32] M.G. Neumann, H.P. Oloveira, A.P.P. Cione, Energy transfer between aromatic hydrocarbons dissolved in a C18-surfactant layer adsorbed on laponite, Adsorption 8 (2002) 141–146.
[33] K. Fujii, N. Iyi, R. Sasai, S. Hayashi, Preparation of a novel luminous heterogeneous system: rhodamine/coumarin/phyllosilicate hybrid and blue shift in fluorescence emission, Chem. Mater. 20 (2008) 2994–3002.
[34] K. Fujii, N. Iyi, H. Hashizume, S. Shimomura, T. Ando, Preparation of integrated coumarin/cyanine systems within an interlayer of phyllosilicate and fluorescence resonance energy transfer, Chem. Mater. 21 (2009) 1179–1181.
[35] T. Kuroda, K. Fujii, K. Sakoda, Ultrafast energy transfer in a multichromophoric layered silicate, J. Phys. Chem. C 114 (2010) 983–989.
[36] N. Kakegawa, A. Yamagishi, Coadsorption studies of tris(1,10-phenanthroline)ruthenium(II) and **N**-methylated alkaloid cation by laponite with an application for a chiral column packing material, Chem. Mater. 17 (2005) 2997–3003.
[37] T. Okada, M. Ogawa, 1,1′-Dimethyl-4,4′-bipyridinium-smectites as a novel adsorbent of phenols from water through charge-transfer interactions, Chem. Commun. (2003) 1378–1379.
[38] D. Madhavan, K. Pitchumani, Efficient triplet-triplet energy transfer using clay-bound ionic sensitizers, Tetrahedron 58 (2002) 9041–9044.
[39] R. Jalubiak, A.H. Francis, Photoinduced electron transfer processes of $CdPS_3$ intercalated with ruthenium tris(bipyridyl) and methylviologen cations, J. Phys. Chem. 100 (1996) 362–367.
[40] C. Devados, P. Bharathi, J.S. Moore, Energy transfer in dendritic macromolecules: molecular size effects and the role of an energy gradient, J. Am. Chem. Soc. 118 (1996) 9635–9644.
[41] C. Giansante, P. Ceroni, M. Venturi, V. Balzani, J. Sakamoto, A.D. Schlüter, Shape-persistent macrocycles functionalized with coumarin dyes: acid-controlled energy- and electron-transfer processes, Chem. Eur. J. 14 (2008) 10772–10781.
[42] S. Su, H. Sasabe, T. Takeda, J. Kido, Pyridine-containing bipolar host materials for highly efficient blue phosphorescent OLEDs, Chem. Mater. 20 (2008) 1691–1693.

[43] N. Miyamoto, Y. Yamada, S. Koizumi, T. Nakato, Extremely stable photoinduced charge separation in a colloidal system composed of semiconducting niobate and clay nanosheets, Angew. Chem. Int. Ed. 46 (2007) 4123–4127.
[44] M. Tsushima, N. Ohta, Electric field effects on photoinduced electron transfer processes of methylene-linked compounds of pyrene and *N,N*-dimethylaniline in a polymer film, J. Chem. Phys. 120 (2004) 6238–6245.
[45] M. Dudič, P. Lhoták, I. Stibor, H. Petříčková, K. Lang, (Thia)calix[4]arene–porphyrin conjugates: novel receptors for fullerene complexation with C_{70} over C_{60} selectivity, New J. Chem. 28 (2004) 85–90.
[46] P.K. Ghosh, A.J. Bard, Photochemistry of tris(2,2′-bipyridyl)ruthenium(II) in colloidal clay suspensions, J. Phys. Chem. 88 (1984) 5519–5526.
[47] J. Chen, S. Li, L. Zhang, B. Liu, Y. Han, G. Yang, Y. Li, Light-harvesting and photoisomerization in benzophenone and norbornadiene-labeled poly(aryl ether) dendrimers via intramolecular triplet energy transfer, J. Am. Chem. Soc. 127 (2005) 2165–2171.
[48] K. Lee, K. Maisel, J.-M. Rouillard, E. Gulari, J. Kim, Sensitive and selective label-free DNA detection by conjugated polymer-based microarrays and intercalating dye, Chem. Mater. 20 (2008) 2848–2850.
[49] V.A. Montes, G.V. Zyryanov, E. Danilov, N. Agarwal, M.A. Palacios, P. Anzenbacher, Ultrafast energy transfer in oligofluorene–aluminum bis(8-hydroxyquinoline)acetylacetone coordination polymers, J. Am. Chem. Soc. 131 (2009) 1787–1795.
[50] G. Olaso-González, M. Merchán, L. Serrano-Anderés, Ultrafast electron transfer in photosynthesis: reduced pheophytin and quinone interaction mediated by conical intersections, J. Phys. Chem. B 110 (2006) 24734–24739.
[51] J.R. Lakowicz, Principles of Fluorescence Spectroscopy, 3rd edition, Springer, New York, 2006.
[52] Th. Förster, Zwischenmolekulare energiewanderung und fluoreszenz, Ann. Phys. (Leipzig Ger.) 437 (1948) 55–75.
[53] D.L. Dexter, A theory of sensitized luminescence in solids, J. Chem. Phys. 21 (1953) 836–850.
[54] G.W. Brindley, G. Brown, Crystal Structure of Clay Minerals and Their X-ray Identification, Mineralogical Society, London, 1984.
[55] K.A. Carrado, P. Thiyagarajan, R.E. Winans, R.E. Botto, Hydrothermal crystallization of porphyrin-containing layer silicates, Inorg. Chem. 30 (1991) 794–799.
[56] K.A. Carrado, Synthetic organo- and polymer-clays: preparation, characterization, and materials applications, Appl. Clay Sci. 17 (2000) 1–23.
[57] K.A. Carrado, R. Csencsits, P. Thiyagarajan, S. Seifert, S.M. Macha, J.S. Harwood, Crystallization and textural porosity of synthetic clay minerals, J. Mater. Chem. 12 (2002) 3228–3237.
[58] Y. Fukushima, M. Tani, An organic/inorganic hybrid layered polymer: methacrylate–magnesium(nickel) phyllosilicate, J. Chem. Soc. Chem. Commun. (1995) 241–242.
[59] Y. Fukushima, M. Tani, Synthesis of 2:1 type 3-(methacryloxy)propyl magnesium(nickel)phyllosilicate, Bull. Chem. Soc. Jpn. 69 (1996) 3667–3671.
[60] M.G. da Fonseca, C.R. Silva, J.S. Barone, C. Airoldi, Layered hybrid nickel phyllosilicates and reactivity of the gallery space, J. Mater. Chem. 10 (2000) 789–795.
[61] M.N. Fernandez-Hernandez, E. Ruiz-Hitzky, Interaction de isocianatos con sepiolite, Clay Mineral. 14 (1979) 295–305.
[62] K. Fujii, S. Hayashi, Hydrothermal syntheses and characterization of alkylammonium phyllosilicates containing $CSiO_3$ and SiO_4 units, Appl. Clay Sci. 29 (2005) 235–248.
[63] K. Fujii, S. Hayashi, H. Kodama, Synthesis of an alkylammonium/magnesium phyllosilicate hybrid nanocomposite consisting of a smectite-like layer and organosiloxane layers, Chem. Mater. 15 (2003) 1189–1197.
[64] K. Fujii, S. Hayashi, Syntheses of smectite-analogue/coumarin composites, in: Proceedings of the 12th International Clay Conference, Elsevier, Amsterdam, The Netherlands, 2003, pp. 443–450.
[65] A. Synak, P. Bojarski, Transition-moment directions of selected carbocyanines from emission anisotropy and linear dichroism measurements in uniaxially stretched polymer films, Chem. Phys. Lett. 416 (2005) 300–304.
[66] L. Scaffardi, P.E. DiPaolo, R. Duchowicz, Simultaneous absorption and fluorescence analysis of the cyanine dye DOCI, J. Photochem. Photobiol. A 107 (1997) 185–188.
[67] M.S. Churio, K.P. Angermund, S.E. Braslavsky, Combination of laser-induced optoacoustic spectroscopy (LIOAS) and semiempirical calculations for the determination of molecular volume changes: the photoisomerization of carbocyanines, J. Phys. Chem. 98 (1994) 1776–1782.
[68] J.C. Kim, Y. Ohga, T. Asano, N.N. Weinberg, A.V. George, Pressure and viscosity effects on thermal geometrical isomerization of oxacarbocyanine cations, Bull. Chem. Soc. Jpn. 74 (2001) 103–111.
[69] M. Maeda, Y. Miyazoe, Flashlamp-excited organic liquid laser in the range from 342 to 889 nm, Jpn. J. Appl. Phys. 11 (1972) 692–698.
[70] A.S. Oliverira, L.F. Vieira Ferreira, D.R. Worrall, F. Wilkinson, Photophysics of oxacyanine dyes on surfaces re-examination of the origins of the 'new emission' observed with laser excitation and high concentrations of adsorbed dyes, J. Chem. Soc. Faraday Trans. 92 (1996) 4809–4814.
[71] Y. Nishikawa, Keikou shigaikyushubunseki, Kyoritsushuppan, Tokyo, 1965.
[72] T. Suratwala, Z. Gardlund, K. Davidson, D.R. Uhlmann, Silylated coumarin dyes in sol–gel hosts. 1. Structure and environmental factors on fluorescent properties, Chem. Mater. 10 (1998) 190–198.
[73] T. Suratwala, Z. Gardlund, K. Davidson, D.R. Uhlmann, Silylated coumarin dyes in sol–gel hosts. 2. Photostability and sol–gel processing, Chem. Mater. 10 (1998) 199–209.
[74] A. Dienes, C.V. Shank, R.L. Kohn, Characteristics of the 4-methylumbelliferone laser dye, IEEE J. Quantum Electron. 9 (1973) 833–843.
[75] SWN has a layered structure consisting of two-dimensional Mg-trioctahedral sheet sandwiched by two Si tetrahedral sheets. Li^+ ion is substituted in part for the octahedral cation sites resulting in negatively charged layers and is located between layers as well to compensate the negative charge. Namely, SWN is hectorite, which is classified into smectite group.
[76] H. Hashizume, S. Shimomura, H. Yamada, T. Fujita, H. Nakazawa, O. Akutsu, An X-ray diffraction system with controlled relative humidity and temperature, Powder Diffr. 11 (1996) 288–289.
[77] G.M. Bilmes, J.O. Tocho, S.E. Braslavsky, Spectrum energy content, and relaxation mechanism of the photoisomer of the laser dye 3,3′-diethyloxadicarbocyanine iodide. Laser-induced optoacoustic studies, J. Phys. Chem. 92 (1988) 5958–5962.
[78] P.F. Aramendía, R.M. Negri, E. San Román, Temperature dependence of fluorescence and photoisomerization in symmetric carbocyanines. Influence of medium viscosity and molecular structure, J. Phys. Chem. 98 (1994) 3165–3173.
[79] S.P. Velsko, H.D. Waldeck, G.R. Fleming, Breakdown of Kramers theory description of photochemical isomerization and the possible involvement of frequency dependent friction, J. Chem. Phys. 78 (1982) 249–258.
[80] I. Baraldi, A. Carnevali, F. Momicchioli, G. Ponterini, Electronic spectra and trans-cis photoisomerism of carbocyanines. A theoretical (CS INDO CI) and experimental study, Spectrochim. Acta A 49 (1993) 471–495.
[81] These spectra are shown in supporting information (Figure S2) with a suitable vertical axis range for these spectra.
[82] S.W. Bailey, Hydrous Phyllosilicates, Mineralogical Society of America, Washington, DC, 1988.
[83] CS Chem3D (Cambridge Soft Corp.) is used for the calculation.
[84] D. Bhattacharjee, S.A. Hussain, S. Chakraborty, R.A. Schoonheydt, Effect of nano-clay platelets on the J-aggregation of thiacyanine dye organized in Langmuir–Blodgett films: a spectroscopic investigation, Spectrochim. Acta A 77 (2010) 232–237.
[85] Y. Kusumoto, H. Sato, K. Maeno, S. Yahiro, Energy transfer dye laser: confirmation of energy transfer by reabsorption effect, Chem. Phys. Lett. 53 (1978) 388–390.
[86] T. Yoshihara, S.I. Druzhinin, K.A. Zachariasse, Fast intramolecular charge transfer with a planar rigidized electron donor/acceptor molecule, J. Am. Chem. Soc. 126 (2004) 8535–8539.
[87] R_0 is given by $R_0 = 0.211[k^2 n^{-4} Q_D J(\lambda)]^{1/6}$ (refer to Ref. [53]), where n is the refractive index of the medium and Q_D is the quantum yield of the donor in the absence of acceptor. k^2 is a factor describing the relative orientation in space of the transition dipoles of the donor and acceptor and is assumed to be typical value (2/3). The overlap integral $J(\lambda)$ express the degree of spectral overlap between the donor emission and the acceptor absorption and is given by $J(\lambda) = \int_0^\infty F_D(\lambda)\varepsilon_A(\lambda)\lambda^4 d\lambda$ (refer to Ref. [53]), where $F_D(\lambda)$ is the corrected fluorescence intensity of the donor in the wavelength range of $\lambda - \lambda + \Delta\lambda$, with the total intensity (area under the curve) normalized to unity, $\varepsilon_A(\lambda)$ is the extinction coefficient of the acceptor at λ.
[88] $I_D(t) = I_D^0 \exp(-t/\tau_D) \exp[-\sigma S(t)]$ where $S(t) = \int_{r_c}^\infty \left\{1 - \exp\left[-\left(\frac{t}{\tau_D}\right)\left(\frac{R_0}{r}\right)^6\right]\right\} 2\pi r\, dr$ τ_D is the decay time of the donor in the absence of an acceptor, σ is the surface density of the acceptor, r_c is the distance of the closest approach between the donor and acceptors, and r is the D–A distance.(refer to Refs. [52,11]).
[89] M. Ogawa, R. Kawai, K. Kuroda, Adsorption and aggregation of a cationic cyanine dye on smectites, J. Phys. Chem. 100 (1996) 16218–16221.
[90] L. Lu, R.M. Jones, D. McBranch, D. Whitten, Surface-enhanced superquenching of cyanine dyes as J-aggregates on laponite clay nanoparticles, Langmuir 18 (2002) 7706–7713.
[91] N. Miyamoto, K. Kuroda, M. Ogawa, Visible light induced electron transfer and long-lived charge separated state in cyanine dye/layered titanate intercalation compounds, J. Phys. Chem. B 108 (2004) 4268–4274.